

# Radio Continuum Emission from the Magnetar SGR J1745-2900: Interaction with Gas Orbiting Sgr A\*

F. Yusef-Zadeh<sup>1</sup>, R. Diesing<sup>1</sup>, M. Wardle<sup>2</sup>, L. O. Sjouwerman<sup>3</sup>, M. Royster<sup>1</sup>,  
W. D. Cotton<sup>4</sup>, D. Roberts<sup>1</sup> & C. Heinke<sup>5</sup>

<sup>1</sup>*CIERA, Department of Physics and Astronomy, Northwestern University, Evanston, IL  
60208*

<sup>2</sup>*Department of Physics and Astronomy, Macquarie University, Sydney NSW 2109,  
Australia*

<sup>3</sup>*National Radio Astronomy Observatory, Socorro, NM 87801*

<sup>4</sup>*National Radio Astronomy Observatory, Charlottesville, VA 22903*

<sup>5</sup>*Department of Physics, University of Alberta, Room #238 CEB, 11322-89 Avenue,  
Edmonton AB T6G 2G7, Canada*

## ABSTRACT

We present radio continuum light curves of the magnetar SGR J1745–2900 and Sgr A\* obtained with multi-frequency, multi-epoch Very Large Array observations between 2012 and 2014. During this period, a powerful X-ray outburst from SGR J1745–2900 occurred on 2013-04-24. Enhanced radio emission is delayed with respect to the X-ray peak by about seven months. In addition, the flux density of the emission from the magnetar fluctuates by a factor of 2 to 4 at frequencies between 21 and 41 GHz and its spectral index varies erratically. Here we argue that the excess fluctuating emission from the magnetar arises from the interaction of a shock generated from the X-ray outburst with the orbiting ionized gas at the Galactic center. In this picture, variable synchrotron emission is produced by ram pressure variations due to inhomogeneities in the dense ionized medium of the Sgr A West bar. The pulsar with its high transverse velocity is moving through a highly blue-shifted ionized medium. This implies that the magnetar is at a projected distance of  $\sim 0.1$  pc from Sgr A\* and that the orbiting ionized gas is partially or largely responsible for a large rotation measure detected toward the magnetar. Despite the variability of Sgr A\* expected to be induced by the passage of the G2 cloud, monitoring data shows a constant flux density and spectral index during this period.

*Subject headings:* Galaxy: center - pulsars: individual (PSR J1745–2900) – stars: magnetars

## 1. Introduction

Detection of pulsars orbiting Sgr A\*, the massive black hole at the Galactic center, is important because they probe the properties of the black hole (Pfahl and Loeb 2004) and the interstellar medium (ISM) of the unique environment of the Galactic center. Magnetars are pulsars with high spin down rate and extremely high inferred magnetic fields ( $10^{14}$  to  $10^{15}$  G) and are generally accompanied by X-ray outbursts. Only four of the 28 known magnetars have exhibited pulsed radio emission (Camilo *et al.* 2006; Levin *et al.* 2010). The recent discovery of the magnetar SGR J1745–2900 has opened a new window to study the ionized medium near Sgr A\*. The Galactic center magnetar was first discovered by *Swift* as an X-ray outburst on JD 2456406 (2013-04-24; Kennea *et al.* 2013). Subsequent X-ray measurements detected pulsed emission with a period of 3.76 s, with a high column density and a small offset from Sgr A\* (e.g., Rea *et al.* 2013; Mori *et al.* 2013). Radio observations detected pulsed emission with a declining spectrum between 4.5 and 20 GHz after the magnetar went into outburst (Shannon and Johnston 2013; Eatough *et al.* 2013; Lynch *et al.* 2015; Torne *et al.* 2015). SGR J1745–2900 has the highest dispersion measure  $DM=1778 \text{ cm}^{-3} \text{ pc}$  and rotation measure  $RM=-6.696 \times 10^4 \text{ rad m}^{-2}$  of any known pulsar in the Galaxy (Shannon and Johnston 2013; Bower *et al.* 2014). These radio measurements suggest that SGR J1745–2900 is likely to be at a projected distance of 0.1 pc from Sgr A\*. Proper motion measurements show a transverse velocity of  $236 \text{ km s}^{-1}$  (Bower *et al.* 2015a) which is consistent with the magnetar being near Sgr A\*.

Using the Jansky Very Large Array (VLA), we recently reported brightening of the continuum emission from the magnetar SGR J1745–2900 at 41 GHz (Yusef-Zadeh *et al.* 2014a). We are motivated to study the light curve of radio emission from the magnetar at high frequencies and its temporal correlation with the X-ray emission. The magnetar has been experiencing a fast decay in its X-ray flux between 3-10 keV followed by a slow decay 200 days after its initial outburst (Rea *et al.* 2013; Coti Zelati *et al.* 2015) on JD 2456406 (2013-04-24). Here, we present light curves of radio emission from the magnetar and Sgr A\*. These radio light curves based on VLA observations show that the onset of enhanced radio emission from the magnetar began seven months after the date of the X-ray outburst. In addition, the light curves of the magnetar indicate that the radio continuum emission at high frequencies fluctuates without an obvious pattern on a monthly time scale. We discuss the time delay between the X-ray outburst and the radio emission in terms of the interaction of an outflow from the magnetar with the material associated with the orbiting ionized gas.

## 2. Observations and Data Reduction

In 2012 October, at the advent of the passage of the G2 cloud with respect to Sgr A\* (e.g., Gillessen *et al.* 2012, Narayan *et al.* 2012), monitoring of the radio flux density of Sgr A\*

began (see Bower *et al.* (2015b) who use the same NRAO service observations data as we do here). Each observation lasted for  $\sim 2$  hours, using up to 2 GHz of continuum bandwidth rotating through the standard observing frequencies centered at 1.5, 3.0, 5.5, 9.0, 14.0, 21.2, 32.02 and 41 GHz. Typical on-source times per frequency setup were about 6 minutes. The flux density was calibrated with respect to 3C286 and bandpass shapes were determined using NRAO530 and 3C286.

The data were calibrated and imaged in AIPS initially and follow-up analysis was made with CASA. To correct for phase instabilities during the scans, phase-only self-calibration was applied (in all observations). Because of the compact nature of both Sgr A\* and the magnetar, we used extended array configurations (A&B) and high frequencies<sup>1</sup>. The absolute flux density of these observations may be inaccurate by up to 10% as the elevation of the primary flux calibrator in most observing runs is far different from that of the Galactic center, introducing errors in modeling the atmospheric transmission at the higher frequencies. These measurements are consistent with millimeter monitoring data indicating a stable flux density of Sgr A\* during the same period (Bower *et al.* 2015b). As the measured flux densities of the magnetar which lies  $2.3''$  SE of Sgr A\*, are tied to the flux density of Sgr A\*, this provides an excellent platform to perform flux density measurements of the magnetar.

We also present the flux density of the magnetar and Sgr A\* from three different epochs of observations on 2011–08–04 (JD2455777), 2014–02–21 (JD 2456710) and 2014-03-09 (JD 2456732). Details of these long observations which were taken in the A configuration are described in Yusef-Zadeh *et al.* (2014b, 2015).

### 3. Results

As part of the long observations of Sgr A\*, we detected a compact source coincident with the magnetar at 34.5 and 44.6 GHz with a flux density of  $1.30 \pm 0.01$  and  $1.62 \pm 0.04$  mJy for an unresolved source on JD 2456732 and 2456710, respectively. The positional offset between SGR 1745-2900 and Sgr A\* is  $2.3917''$  and  $2.3923''$  with statistical errors of 1.9 and 1.1 mas accuracy at 44.6 and 34 GHz, respectively, and systematic errors of few mas. The comparison of the continuum radio emission from the magnetar with earlier long VLA observations taken on JD 2455777 (2011-08-04), with similar resolution and sensitivity, indicate that the magnetar has brightened significantly at 42 GHz. The magnetar was not detected above  $3\sigma \sim 243 \mu\text{Jy beam}^{-1}$  at 42 GHz on JD 2455777. The flux has increased by at least a factor of 7 between these two epochs. Figure 1a, which is based on data taken over a long observation on 2014-03-09 (JD 2456732), shows a 34 GHz continuum image of the  $6'' \times 3''$  region of the ionized gas surrounding Sgr A\* and SGR J1745–2900 with a spatial resolution of  $0.1''$ . The magnetar, as labeled on this figure, is projected to the SE of Sgr A\* and at the edge of a shell-like ionized feature. The ionized medium surrounding the magnetar has a high density of  $10^{4-5} \text{ cm}^{-3}$  and a highly blue-shifted velocity  $-200 \text{ km s}^{-1}$  with broad linewidth (e.g., Roberts *et al.* 1996; Zhao *et al.* 2009). This complex region shows a wide

---

<sup>1</sup><https://science.nrao.edu/science/service-observing>

range of angular scales including an elongated cavity of ionized gas with surface brightness  $\sim 15 \mu\text{Jy beam}^{-1}$  at 34 GHz to the NE of the magnetar extending for  $\sim 1.5''$ .

We used the snapshot monitoring data taken with the VLA at the highest available frequency bands (K, Ka and Q) in the most extended configurations (A & B). Figure 1b–d show three images of the medium surrounding the magnetar at 41 GHz based on snapshot observations taken on JD 2456626, 2456656 and 2456704, respectively. The magnetar is detected with a signal-to-noise  $\sim 26$  in the snapshot observation taken on JD 2456704. The flux densities of the magnetar and Sgr A\* are determined in the image plane by fitting a 2D Gaussian to individual sources. The parameters of the fit to both long and short observations are listed in Table 1 with entries in columns 1 to 7 corresponding to the observation calendar date, the observing date in JD, the observing center frequency, the magnetar and Sgr A\* flux densities, the VLA array configuration and the synthesized beam, respectively. The flux density of Sgr A\* is relatively constant with a typical flux density  $\sim 1.5$  Jy at 41 GHz.

Figure 2a shows the light curves of the magnetar and Sgr A\* in blue and red colors, respectively. Because the VLA was in its compact configuration (C & D), the emission from the magnetar during days JD 2456350 and JD 2456550 is assumed to be similar to the upper limits given in Figure 2a between JDs 2456250 and 2456550. The emission from the magnetar is not detected until JD 2456710 and then fluctuates in all bands by a factor of 2 to 4 between epochs. Our B-array data taken at 41 GHz (Fig. 1b,c and the bottom panel of Fig. 2a) show  $3\sigma$  upper limits of 0.82 (JD 2456592) and 0.70 (JD 2456626) mJy beam $^{-1}$ . These values are less than the flux density  $1.85 \pm 0.07$  detected in the A configuration on JD 2456704 at 41 GHz. The upper limit on JD 2456656 is too high to distinguish the magnetar from the diffuse emission. Thus, these observations show that the magnetar was not detected at 41 GHz until JD 2456626, seven months after the X-ray outburst occurred. It is possible that we did not detect radio emission prior to this period because of our poor sensitivity, though our measurements are not inconsistent with the 8.7 GHz monitoring data indicating that the flux density of the pulsar became stronger and more erratic after JD 2456726 (Lynch *et al.* 2015).

The variable fluxes of the magnetar and Sgr A\* as a function of frequency are shown in Figure 2b. Unlike the constant spectral index of Sgr A\*, the magnetar shows an erratic spectral index. Table 2 provides the values of the spectral index  $\alpha$  where the flux density is  $F_\nu \propto \nu^\alpha$  for three pairs of frequencies. Entries in column 1 to 5 of Table 2 give the calendar date, JD, the spectral index between 21 and 32 GHz, 32 and 41 and 21 and 41 GHz, respectively. The erratic and steady spectral index values of the magnetar and Sgr A\*, respectively, are noted in column 3, 4 and 5. Torne *et al.* 2015) have recently shown significant flux variations on timescales of the order of tens of minutes. Since this timescale is not much longer than the on-source time per frequency setup in our data (6 minutes), it is possible that there may have been intrinsic evolution in the radio flux between observations at different frequencies, making it hard to interpret the measured spectral indices.

Pulsed radio emission from the magnetar SGR J1745–2900 was reported to have a flux density of 0.3 mJy beam $^{-1}$  at  $\nu=18$  GHz with a decreasing flux density at higher frequencies on 2013-05-01 (Shannon & Johnson 2013). Using the spectral index of  $\alpha = -1$ , the expected

flux density of pulsed emission at 42 GHz is  $0.12 \text{ mJy beam}^{-1}$ ,  $\sim 7\%$  of the flux density detected at 44 GHz, assuming that the magnetar was not showing variable emission. It turned out that monitoring of the magnetar with the GBT indicated that the magnetar underwent a dramatic change in flux density and pulse profile morphology at 8.7 GHz near JD 2456713 (Lynch *et al.* 2015). Enhanced 44 GHz emission was also detected, as shown in Figure 2a, during this epoch. The GBT observations show also an erratic behavior of pulsed radio emission at 8.7 GHz. More recently, Torne *et al.* (2015) report the detection of pulsed emission up to 245 GHz. These measurements are consistent with our high frequency, high resolution 41 GHz continuum data. It is possible that the high frequency emission is entirely due to pulsed emission (Torne *et al.* 2015). We have an alternate picture in which the unpulsed emission from the shock front could contribute to the total high frequency radio emission.

#### 4. Discussion & Conclusion

The emission from the magnetar is pulsed at radio wavelengths with a nonthermal spectrum. Here we propose an additional unpulsed component that originates from a shock front and could contribute to radio and X-ray emission. We argue that an increase in the continuum flux at high frequencies could in part be explained by the magnetar’s winds interacting with the ionized gas orbiting around Sgr A\*. The magnetar is moving with a high transverse velocity of  $236 \text{ km s}^{-1}$  (Bower *et al.* 2015a) with a position angle (PA)  $\sim 22^\circ$  through a highly blue shifted  $-200 \text{ km s}^{-1}$  ionized medium (Roberts *et al.* 1996; Zhao *et al.* 2009). The ionized gas associated with Sgr A West has a transverse velocity that is opposite to that of the magnetar (Yusef-Zadeh *et al.* 1998; Zhao *et al.* 2009). This interaction will create a bow shock assuming that the magnetar is embedded within the bar of orbiting ionized gas, at a projected distance of 0.1 pc from Sgr A\*. This would then strengthen the suggestion that the magnetar is at the Galactic center (Bower *et al.* 2015a).

We hypothesize that the magnetar’s radio emission is in part produced by synchrotron emission from electrons accelerated in a reverse shock arising from the interaction of a pulsar’s outflow – perhaps expanded significantly by the magnetar’s outburst – with the dense ionized material in the Sgr A West bar. To estimate the properties of the cometary bubble predicted in this model, we characterize the source region by radius  $R$ , and assume that it is threaded by a uniform magnetic field  $B$ , and that the relativistic electrons between 1 MeV and 10 GeV are in equipartition with the magnetic field and have a power-law energy spectrum  $\propto E^{-1}$ , producing a flat synchrotron spectrum. Then the synchrotron flux is

$$S_\nu \approx 0.67 \left( \frac{R}{2 \times 10^{14} \text{ cm}} \right)^3 \left( \frac{B}{0.1 \text{ G}} \right)^{7/2} \text{ mJy} \quad (1)$$

where we have adopted a distance of 8 kpc to the Galactic center. Equating twice the magnetic pressure in the source, i.e.  $B^2/4\pi$ , to the incident ram pressure due to relative motion of the magnetar and the surrounding ionized interstellar gas,  $P_{\text{ram}} = \rho v_{\text{rel}}^2$ , we obtain

$$S_\nu \approx 3.4 \left( \frac{R}{2 \times 10^{14} \text{ cm}} \right)^3 \left( \frac{n_H}{10^5 \text{ cm}^{-3}} \right)^{7/2} \left( \frac{v_{\text{rel}}}{1000 \text{ km s}^{-1}} \right)^{7/4} \text{ mJy} \quad (2)$$

This implies a source diameter of roughly 20 AU, equivalent to 2.5 mas at 8 kpc. The pressure in the cometary bubble supported by the outflow must also be comparable to the external ram pressure, implying an energy content  $E_{\text{bubble}} = (3P_{\text{ram}}) \times (4/3\pi R^3) \approx 2.4 \times 10^{41}$  erg for the reference values in equation (2). The magnetar spin down rate implies  $\dot{E} = 1.3 \times 10^{34}$  erg s<sup>-1</sup> (Lynch et al. 2015) so this energy can be replaced on a time scale of about 6 months. Variability of the synchrotron emission may be produced by ram pressure variations due to inhomogeneities in the external medium: increased ram pressure compresses the cometary outflow bubble ( $R \propto P_{\text{ram}}^{-3/4}$ ) and increases the field strength in the synchrotron source region ( $B \propto P_{\text{ram}}^{1/2}$ ); equation (2) implies that  $S_\nu \propto P_{\text{ram}}$ . In this picture, the outflow produces a 20 AU bubble with the mean expansion speed of  $\sim 170$  km s<sup>-1</sup>, seven months after the X-ray outburst when the magnetar becomes radio loud at high frequencies.

This model can also explain the spectral index of the emission from the magnetar. For optically thin synchrotron radio emission, the energy index  $p=2$  where  $\alpha = (1 - p)/2$ . For different values of the spectral index, the spectrum becomes flat or inverted when the emission becomes optically thick. Diffusive shock acceleration by a single shock is known to produce a power-law energy distribution with  $\alpha=0.5$  (Blandford & Eichler 1987). However, multiple, identical and nonidentical shocks can produce a varying degree of spectral index including a flat spectrum (Pope & Melrose 1994; Melrose & Pope 1993). In the context of this model, the synchrotron emission from the bow shock should also be polarized at radio wavelengths if the magnetic field is not tangled. The direction of the magnetic field in the optically thin synchrotron source is likely to be parallel to the bow shock. Recent polarization measurements show that the intrinsic PA of the electric field is  $\sim 16 \pm 9^\circ$  (Kravchenko *et al.* 2015), which is well within the PA of the proper motion of the magnetar (Bower *et al.* 2015a). This polarization result is not inconsistent with the expected magnetic field direction in the shock front.

In addition to nonthermal radio emission, the dense interstellar gas is shock-heated to temperatures  $\sim 1.4 \times 10^7 v_{\text{rel}}^2$  K as it collides with the outflow bubble, and subsequently emits X-rays while flowing around the obstruction and expanding downstream. The radiative cooling time is about 15 years, so the gas cools primarily by adiabatic expansion on a time scale  $t_{\text{exp}} = R/c_s \sim 0.1$  yr, where  $c_s$  is the sound speed in the post-shock gas. We estimate the 2–8 keV luminosity of the shocked gas using

$$L_X \approx \pi(2R)^2 \frac{1}{4} v_{\text{rel}} t_{\text{exp}} \times (4n_{\text{H}})^2 \Lambda(T) \times [e^{-2 \text{ keV}/kT} - e^{-8 \text{ keV}/kT}] \quad (3)$$

where the three factors are the volume of hot shocked gas (determined using twice the radius of the synchrotron source which itself is estimated for a 30 GHz radio flux of 3 mJy using equation (2), its cooling rate per unit volume, and, lastly, the fraction of radiation emitted in the 2–8 keV window. The factors of four account for the compression of the gas as it is shocked. We adopt an approximation to the cooling function computed by Böhringer and Hensler (1989) for twice solar metallicity:  $\Lambda(T) = 1.5 ([0.4/T_7]^{2.75} + [T_7/0.4]^{0.8})$  for  $0.2 < T_7 \leq 11$ , or  $1.2 ([1.5/T_7]^{1.4} + T_7^{0.5})$  for  $T_7 > 1$  in units of  $10^{-23}$  erg cm<sup>3</sup> s<sup>-1</sup>, where  $T_7 = T/10^7$  K. We plot the resulting luminosity in Figure 3 as a function of the assumed relative velocity between the magnetar and the dense ionized material associated with Sgr A West. We note that the flux is three orders of magnitude below the current X-ray flux of the magnetar (e.g.

Kaspi et al 2014), and so is not currently observable. However, because of its quadratic dependence on the size of the source, the X-ray luminosity could be detected in the future if the emitting region were ten times larger.

The emission measure of the ionized gas in Sgr A West in the vicinity of the magnetar is  $n_e^2 L \approx 2 \times 10^7 \text{ cm}^{-6} \text{ pc}$  (e.g. Roberts *et al.* 1996; Zhao *et al.* 2009), yielding  $\text{RM} \approx 8 \times 10^4 B_{0.5\text{mG}}/n_5 \text{ rad m}^{-2}$ . This value is very similar to the observed value if the magnetic field is 0.5 mG and the electron density  $10^5 \text{ cm}^{-3}$ . Using dust polarization measurements, Aitken *et al.* (1998) estimated a minimum magnetic field of  $\sim 2$  mG in the bar of ionized gas. Our value of the magnetic field is reasonable when compared to those of Aitken et al. (1998). Thus the ionized orbiting gas is likely responsible for the observed high rotation measure,  $\text{RM} \approx -6.7 \times 10^4 \text{ rad m}^{-2}$ . Unlike the warm ionized medium within a few tenths of Sgr A\* proposed here, another recent study of the RM of the magnetar suggests that the hot X-ray emitting gas within several parsecs of Sgr A\* is responsible for the high RM (Eatough *et al.* 2013).

In summary, we presented light curves of the magnetar and Sgr A\* over the course of the monitoring campaign as the G2 cloud approached Sgr A\*. We find that the flux density and the spectral index of Sgr A\* remained constant whereas the continuum emission and the spectral index of the magnetar showed an erratic behavior similar to that of its pulsed emission (Lynch *et al.* 2015). We noted high frequency 44 GHz emission was detected about seven months after the X-ray outburst. We argued that this time delay and the enhanced radio emission from the magnetar could be explained by the interaction of the wind from the magnetar with the orbiting ionized gas near Sgr A\*. This picture can also explain the large RM observed toward the magnetar implying that the Faraday screen is localized within the ionized layer orbiting Sgr A\*. The continuum radio emission arises from two components, pulsed and unpulsed emission. The relationship of the pulsed and shocked emission remains unclear. Future observations are required to determine the contribution of shocked emission.

Acknowledgments: We thank the referee for useful comments. This work is partially supported by the grant AST-1517246 from the NSF. The authors wish to thank the NRAO staff for instigating the service monitoring observations and, in particular, Claire Chandler for providing the calibrated data and images. The National Radio Astronomy Observatory is a facility of the National Science Foundation operated under cooperative agreement by Associated Universities, Inc.

## REFERENCES

- Aitken, D. K., Smith, C. H., Moore, T. J. T., & Roche, P. F. 1998, MNRAS, 299, 743
- Blandford, R., & Eichler, D. 1987, Phys. Rep., 154, 1
- Böhringer, H. & Hensler, G. 1989, A&A, 215, 147
- Bower, G. C., Deller, A., Demorest, P., et al. 2014, ApJ, 780, L2
- Bower, G. C., Deller, A., Demorest, P., et al. 2015a, ApJ, 798, 120

- Bower, G. C., Markoff, S., Dexter, J., et al. 2015b, *ApJ*, 802, 69
- Camilo, F., Ransom, S. M., Halpern, J. P., et al. 2006, *Nature*, 442, 892
- Coti Zelati, F., Rea, N., Papitto, A., et al. 2015, *MNRAS*, 449, 2685
- Gillessen, S., Genzel, R., Fritz, T. K., et al. 2012, *Nature*, 481, 51
- Eatough, R. P., Falcke, H., Karuppusamy, R., et al. 2013, *Nature*, 501, 391
- Kennea, J. A., Burrows, D. N., Kouveliotou, C., et al. 2013, *ApJ*, 770, L24
- Levin, L., Bailes, M., Bates, S., et al. 2010, *ApJ*, 721, L33
- Lynch, R. S., Archibald, R. F., Kaspi, V. M., & Scholz, P. 2015, *ApJ*, 806, 266
- Melrose, D. B., & Pope, M. H. 1993, *Proceedings of the Astronomical Society of Australia*, 10, 222
- Mori, K., Gotthelf, E. V., Zhang, S., et al. 2013, *ApJ*, 770, L23
- Narayan, R., Özel, F., & Sironi, L. 2012, *ApJ*, 757, L20
- Pfahl, E., & Loeb, A. 2004, *ApJ*, 615, 253
- Pope, M. H., & Melrose, D. B. 1994, *Proceedings of the Astronomical Society of Australia*, 11, 175
- Rea, N., Esposito, P., Pons, J. A., et al. 2013, *ApJ*, 775, L34
- Roberts, D. A., Yusef-Zadeh, F., & Goss, W. M. 1996, *ApJ*, 459, 627
- Shannon, R. M., & Johnston, S. 2013, *MNRAS*, 435, L29
- Torne, P., Eatough, R. P., Karuppusamy, R., et al. 2015, *MNRAS*, 451, L50
- Yusef-Zadeh, F., Roberts, D., Heinke, C., et al. 2014, *The Astronomer’s Telegram*, 6041, 1
- Yusef-Zadeh, F., Roberts, D. A., & Biretta, J. 1998, *ApJ*, 499, L159
- Yusef-Zadeh, F., Roberts, D. A., Bushouse, H., et al. 2014, *ApJ*, 792, L1
- Yusef-Zadeh, F., Roberts, D. A., Wardle, M., et al. 2015, *ApJ*, 801, L26
- Zhao, J.-H., Morris, M. R., Goss, W. M., & An, T. 2009, *ApJ*, 699, 186



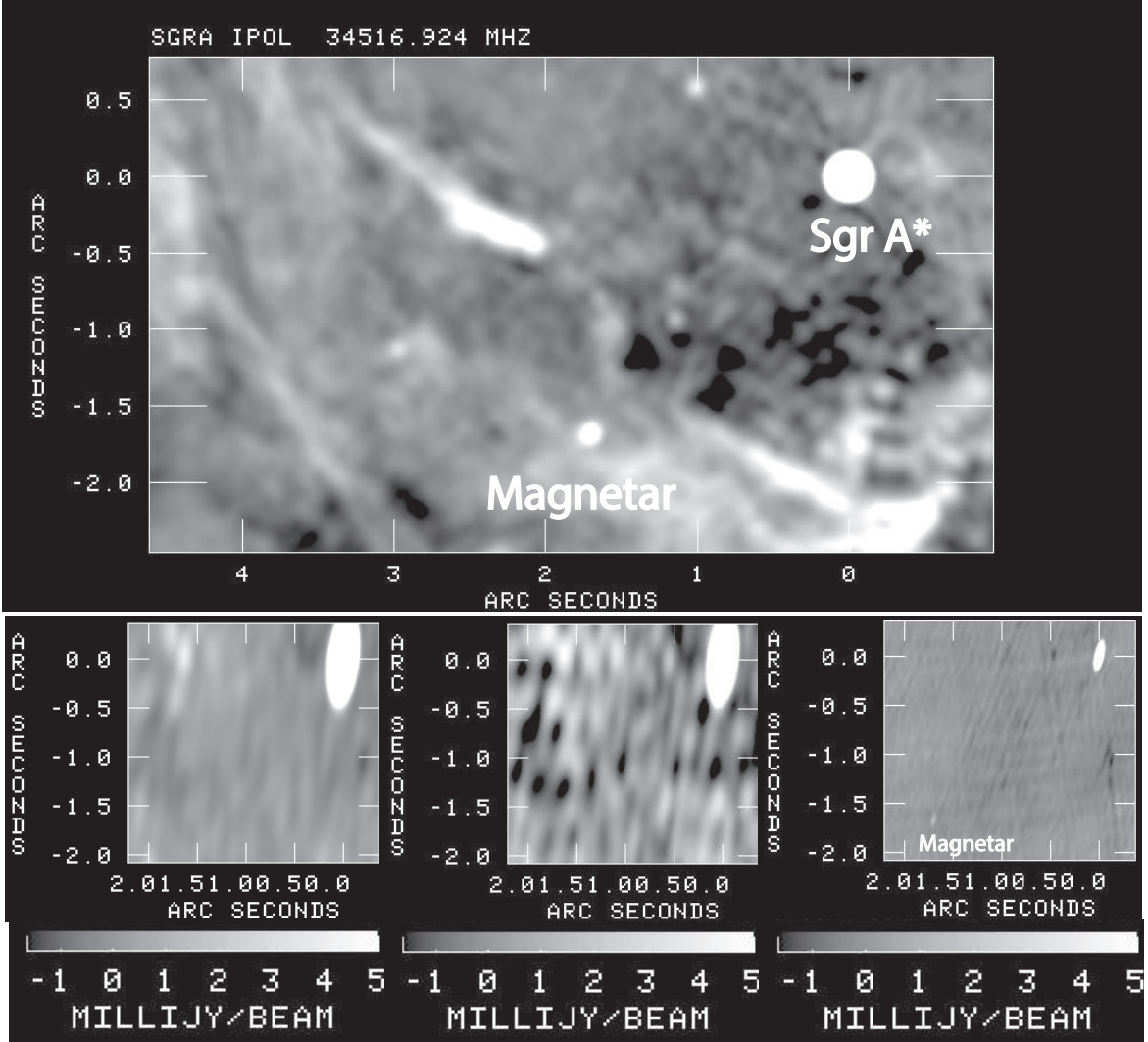


Fig. 1.— (a) *Top* A grayscale continuum image of the region surrounding the magnetar SGR J1740-2900 at 34 GHz taken on JD 2456732 (2014-03-09) convolved to a resolution of  $0.1''$ . The grayscale ranges between  $-0.13$  and  $1 \text{ mJy beam}^{-1}$ . (b–d) *Bottom* Three 41 GHz images from left to right are based on short observations on JD 2456626 (2013-11-29), JD 2456656 (2013-12-29) and JD 2456704 (2014-2-15), respectively. The right image shows the detection of the magnetar (see Table 1). The display range is between  $-1.59$  and  $5 \text{ mJy}$  for all three images.

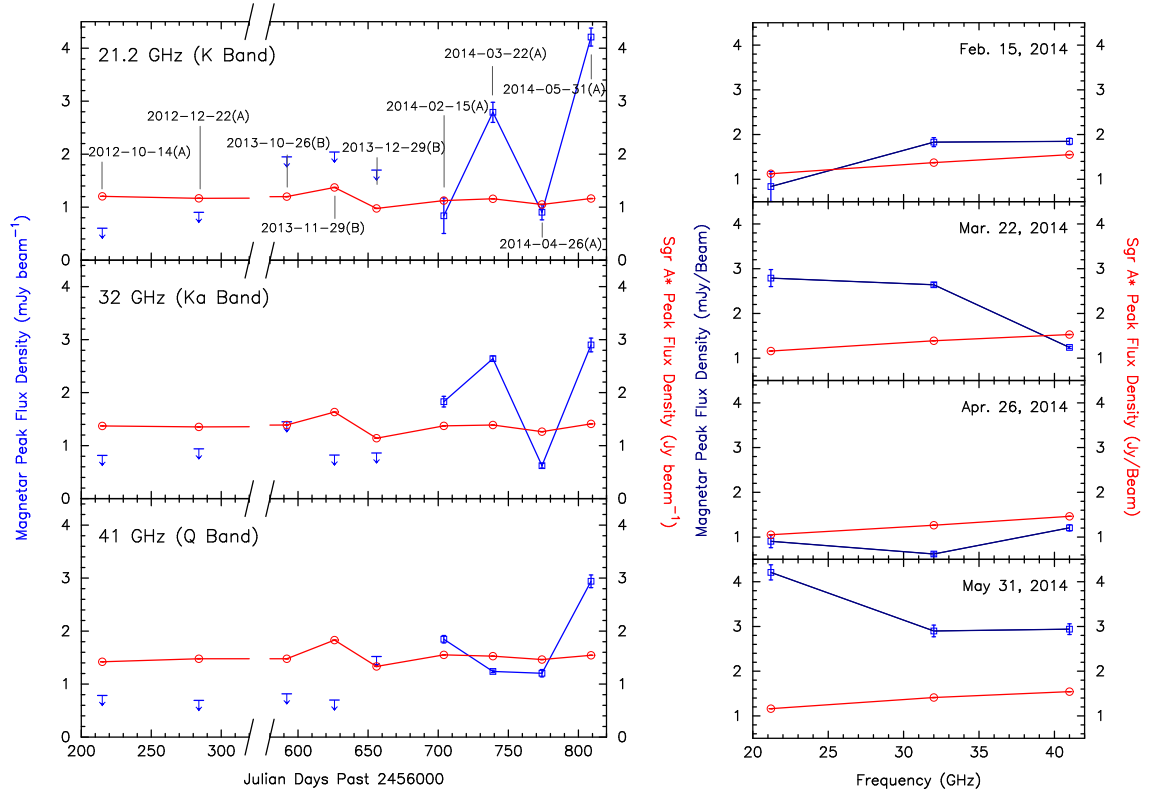


Fig. 2.— (a) *Top* Light curves of the magnetar and Sgr A\* are shown in blue squares and red circles, respectively. Four epochs of observations are plotted at three different frequencies: 21.2, 32 and 41 GHz, corresponding to K, Ka, Q bands, respectively. The arrows give  $3\sigma$  upper limits of the flux density of the magnetar. Note that the flux density scale is in mJy beam<sup>-1</sup> for the magnetar (blue, left hand side) and is in Jy beam<sup>-1</sup> (red, right hand side) for Sgr A\*. The dashed line coincides with JD 2456406 when the magnetar went into an X-ray outburst. Only snapshot observations are used. (b) *Bottom* Similar to (a) except that the flux densities of the magnetar and Sgr A\* are given as function of frequency.

Table 1. The Flux Densities of Sgr A\* and SGR J1745–2900

Date	JD	Frequency (GHz)	Magnetar Flux (mJy)	Sgr A* Flux <sup>b</sup> (Jy)	Configuration (VLA)	Beam ( $\theta''_a \times \theta''_b$ (PA $^\circ$ ))
2011-08-04	2455777 <sup>c</sup>	42	< 0.24 <sup>a</sup>	2.18	A	0.08 $\times$ 0.04 (-5.5)
2012-10-14	2456215	21.2	< 0.60 <sup>a</sup>	1.20	A	0.20 $\times$ 0.06 (5.7)
2012-10-14	2456215	32	< 0.81 <sup>a</sup>	1.37	A	0.13 $\times$ 0.04 (-177.6)
2012-10-14	2456215	41	< 0.78 <sup>a</sup>	1.42	A	0.11 $\times$ 0.03 (-178.8)
2012-12-22	2456284	21.2	< 0.90 <sup>a</sup>	1.17	A	0.20 $\times$ 0.06 (9.0)
2012-12-22	2456284	32	< 0.94 <sup>a</sup>	1.35	A	0.13 $\times$ 0.05 (-15.5)
2012-12-22	2456284	41	< 0.69 <sup>a</sup>	1.47	A	0.11 $\times$ 0.03 (-13.5)
2013-10-26	2456592	21.2	< 1.95 <sup>a</sup>	1.20	B	0.66 $\times$ 0.20 (12.7)
2013-10-26	2456592	32	< 1.45 <sup>a</sup>	1.39	B	0.46 $\times$ 0.13 (9.7)
2013-10-26	2456592	41	< 0.82 <sup>a</sup>	1.48	B	0.34 $\times$ 0.10 (7.8)
2013-11-29	2456626	21.2	< 2.04 <sup>a</sup>	1.37	B	0.67 $\times$ 0.19 (-2.1)
2013-11-29	2456626	32	< 0.82 <sup>a</sup>	1.63	B	0.44 $\times$ 0.13 (-4.0)
2013-11-29	2456626	41	< 0.70 <sup>a</sup>	1.83	B	0.34 $\times$ 0.11 (-6.1)
2013-12-29	2456656	21.2	< 1.70 <sup>a</sup>	0.98	B	0.65 $\times$ 0.20 (-2.1)
2013-12-29	2456656	32	< 0.861 <sup>a</sup>	1.14	B	0.44 $\times$ 0.13 (-4.2)
2013-12-29	2456656	41	< 1.52 <sup>a</sup>	1.33	B	0.34 $\times$ 0.11 (-6.8)
2014-02-15	2456704	21.2	0.84 $\pm$ 0.33	1.12	A	0.20 $\times$ 0.06 (-7.6)
2014-02-15	2456704	32	1.83 $\pm$ 0.10	1.37	A	0.13 $\times$ 0.04 (-9.7)
2014-02-15	2456704	41	1.85 $\pm$ 0.07	1.55	A	0.11 $\times$ 0.03 (-11.8)
2014-02-21	2456710 <sup>c</sup>	44.6	1.62 $\pm$ 0.04	1.49	A	0.07 $\times$ 0.03 (-4.0)
2014-03-09	2456732 <sup>c</sup>	34.5	1.30 $\pm$ 0.01	1.72	A	0.08 $\times$ 0.05 (-1.56)
2014-03-22	2456739	21.2	2.79 $\pm$ 0.19	1.16	A	0.20 $\times$ 0.06 (10.6)
2014-03-22	2456739	32	2.64 $\pm$ 0.05	1.39	A	0.19 $\times$ 0.04 (8.3)
2014-03-22	2456739	41	1.24 $\pm$ 0.02	1.53	A	0.10 $\times$ 0.033 (5.1)
2014-04-26	2456744	21.2	0.90 $\pm$ 0.14	1.05	A	0.20 $\times$ 0.06 (0.9)
2014-04-26	2456744	32	0.62 $\pm$ 0.04	1.26	A	0.13 $\times$ 0.04 (-1.0)
2014-04-26	2456744	41	1.20 $\pm$ 0.07	1.46	A	0.10 $\times$ 0.03 (-3.5)
2014-05-31	2456809	21.2	4.21 $\pm$ 0.17	1.16	A	0.23 $\times$ 0.06 (-177.6)
2014-05-31	2456809	32	2.90 $\pm$ 0.13	1.41	A	0.15 $\times$ 0.05 (-2.3)
2014-05-31	2456809	41	2.94 $\pm$ 0.12	1.54	A	0.13 $\times$ 0.03 (-4.1)

<sup>a</sup>3 $\sigma$  upper limit

<sup>b</sup>1 $\sigma$  error is < 0.1%

<sup>c</sup>long observations

Table 2. Spectral Index of SGR J1745–2900 and Sgr A\*

Date	JD	$\alpha_1$ (32–21.2 GHz)	$\alpha_2$ (41–32 GHz)	$\alpha_3$ (41–21.2 GHz)
Magnetar				
2014-02-15	2456704	1.89 $\pm$ 0.95	0.04 $\pm$ 0.20	1.20 $\pm$ 0.75
2014-03-22	2456739	-0.13 $\pm$ 0.17	-3.05 $\pm$ 0.08	-1.23 $\pm$ 0.13
2014-04-26	2456744	-0.91 $\pm$ 0.41	2.67 $\pm$ 0.28	0.43 $\pm$ 0.31
2014-05-31	2456809	-0.90 $\pm$ 0.14	0.05 $\pm$ 0.18	-0.54 $\pm$ 0.11
Sgr A*				
2014-02-15	2456704	0.49 $\pm$ 0.00	0.49 $\pm$ 0.00	0.49 $\pm$ 0.00
2014-03-22	2456739	0.44 $\pm$ 0.00	0.38 $\pm$ 0.00	0.42 $\pm$ 0.00
2014-04-26	2456744	0.45 $\pm$ 0.00	0.59 $\pm$ 0.00	0.50 $\pm$ 0.00
2014-05-31	2456809	0.47 $\pm$ 0.00	0.36 $\pm$ 0.00	0.43 $\pm$ 0.00

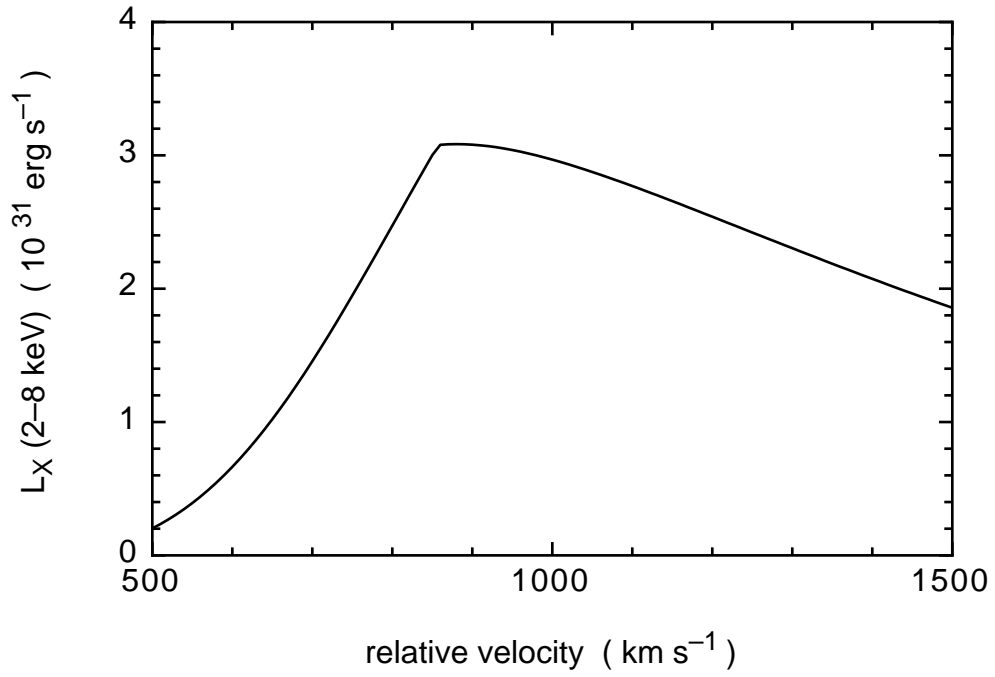


Fig. 3.— Thermal X-ray luminosity produced from the ISM shocked by the relative motion of the magnetar and the material in Sgr A West, assuming that the synchrotron radio flux at 30 GHz is 3 mJy (see text).